However there is a lower limit to λ determined by the need to supply the α/β interfacial energy, $\gamma_{\alpha\beta}$.

For an interlamellar spacing, λ, there is a total of $(2/\lambda)$ m^2 of α/β interface per m^3 of eutectic. Thus the free energy change associated with the solidification of 1 mol of liquid is given by

$$\Delta G(\lambda) = -\Delta G(\infty) + \frac{2\gamma_{\alpha\beta}V_m}{\lambda} \tag{4.37}$$

where V_m is the molar volume of the eutectic and $\Delta G(\infty)$ is the free energy decrease for very large values of λ. Since solidification will not take place if $\Delta G(\lambda)$ is positive, $\Delta G(\infty)$ must be large enough to compensate for the interfacial energy term, i.e. the eutectic/liquid interface must be undercooled below the equilibrium eutectic temperature T_E, Fig. 4.32. If the total undercooling is ΔT_0 it can be shown that $\Delta G(\infty)$ is then given approximately by

$$\Delta G(\infty) = \frac{\Delta H \cdot \Delta T_0}{T_E} \tag{4.38}$$

where ΔH is an enthalpy term. The minimum possible spacing (λ^*) is obtained by using the relation $\Delta G(\lambda^*) = 0$, whence

$$\lambda^* = \frac{2\gamma_{\alpha\beta}V_m T_E}{\Delta H \cdot \Delta T_0} \tag{4.39}$$

When the eutectic has this spacing the free energy of the liquid and eutectic is the same, i.e. all three phases are in equilibrium. This is because the α/β interface raises the free energies of the α and β from $G^\alpha(\infty)$ and $G^\beta(\infty)$ to $G^\alpha(\lambda^*)$ and $G^\beta(\lambda^*)$ as shown in Fig. 4.32. The cause of the increase is the curvature of the α/L and β/L interfaces arising from the need to balance the interfacial tensions at the α/β/L triple point, Fig. 4.31. In general, therefore, the increase will be different for the two phases, but for simple cases it can be shown to be $2\gamma_{\alpha\beta}V_m/\lambda$ for both, Fig. 4.32.

Let us now turn to the mechanism of growth. If solidification is to occur at a finite rate there must be a flux of atoms between the tips of the α and β lamellae and this requires a finite composition difference. For example the concentration of B must be higher ahead of the α phase than ahead of the β phase so that B rejected from the α can diffuse to the tips of the growing β. If $\lambda = \lambda^*$ growth will be infinitely slow because the liquid in contact with both phases has the same composition, X_E in Fig. 4.32. However if the chosen spacing is greater than λ^* less free energy is locked in the interfaces and G^α and G^β are correspondingly reduced, Fig. 4.33a. Under these circumstances the liquid in local equilibrium with the α has a composition $X_B^{L/\alpha}$ which is richer in B than the composition in equilibrium with the β phase $X_B^{L/\beta}$.

If the α/L and β/L interfaces are highly mobile it is reasonable to assume that growth is diffusion controlled in which case the eutectic growth rate (v) should be proportional to the flux of solute through the liquid. This in turn will vary as $D\,dC/dl$ where D is the liquid diffusivity and dC/dl is the

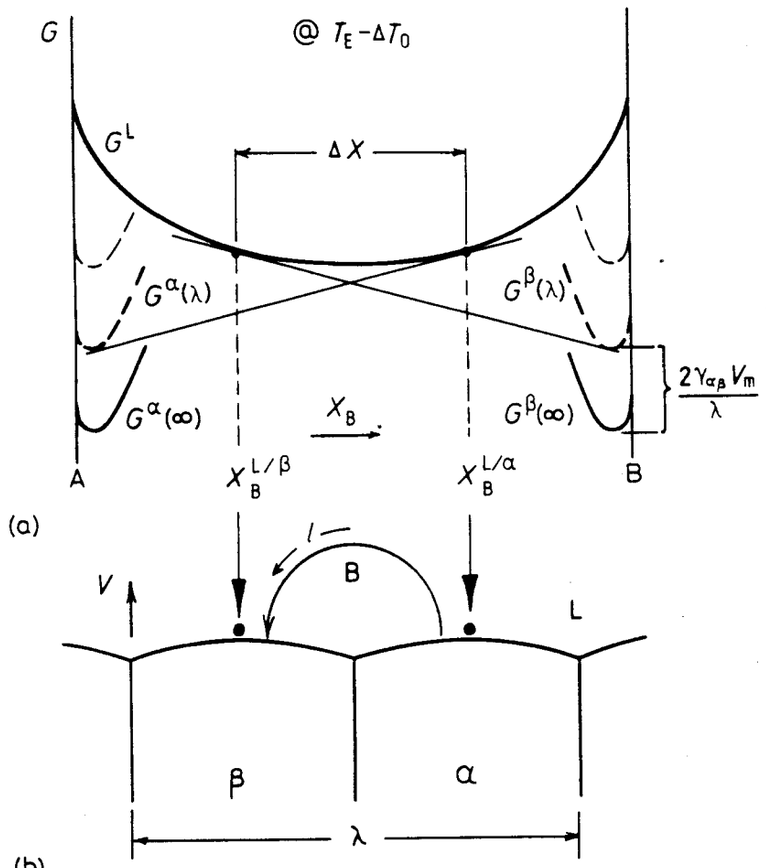

Fig. 4.33 (a) Molar free energy diagram at $(T_E - \Delta T_0)$ for the case $\lambda^* < \lambda < \infty$, showing the composition difference available to drive diffusion through the liquid (ΔX). (b) Model used to calculate the growth rate.

concentration gradient driving the diffusion. (l is measured along the direction of diffusion as shown in Fig. 4.33b. In practice dC/dl will not have a single value but will vary from place to place within the diffusion zone.) dC/dl should be roughly proportional to the maximum composition difference $(X_B^{L/\alpha} - X_B^{L/\beta})$ and inversely proportional to the effective diffusion distance, which, in turn, will be linearly related to the interlamellar spacing (λ). Thus we can write

$$v = k_1 D \frac{\Delta X}{\lambda} \tag{4.40}$$

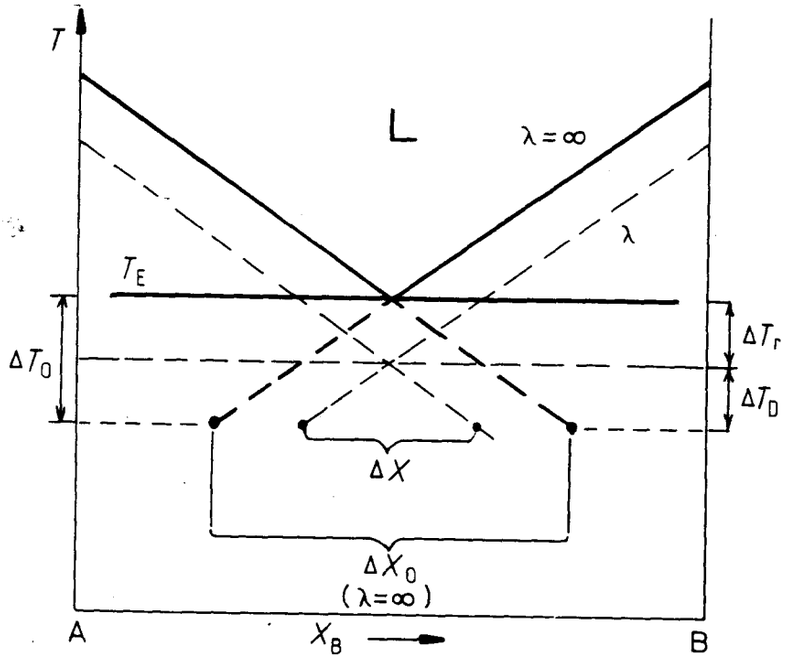

Fig. 4.34 Eutectic phase diagram showing the relationship between ΔX and ΔX_0 (exaggerated for clarity).

where k_1 is a proportionality constant and $\Delta X = X_B^{L/\alpha} - X_B^{L/\beta}$ as given in Fig. 4.33.

ΔX will itself depend on λ for when $\lambda = \lambda^*$, $\Delta X = 0$, and as λ increases ΔX will tend to a maximum value, ΔX_0, say. Therefore it is reasonable to write

$$\Delta X = \Delta X_0\left(1 - \frac{\lambda^*}{\lambda}\right) \tag{4.41}$$

The magnitude of ΔX_0 can be obtained by extrapolating the equilibrium liquidus lines of the phase diagram ($\lambda = \infty$) as shown in Fig. 4.34. For small undercoolings

$$\Delta X_0 \propto \Delta T_0 \tag{4.42}$$

The dashed lines in Fig. 4.34 are the liquidus lines for $\lambda^* < \lambda < \infty$. ΔX is simply given by the extrapolation of these lines as shown. Combining the above equations gives

$$v = k_2 D \Delta T_0 \frac{1}{\lambda}\left(1 - \frac{\lambda^*}{\lambda}\right) \tag{4.43}$$

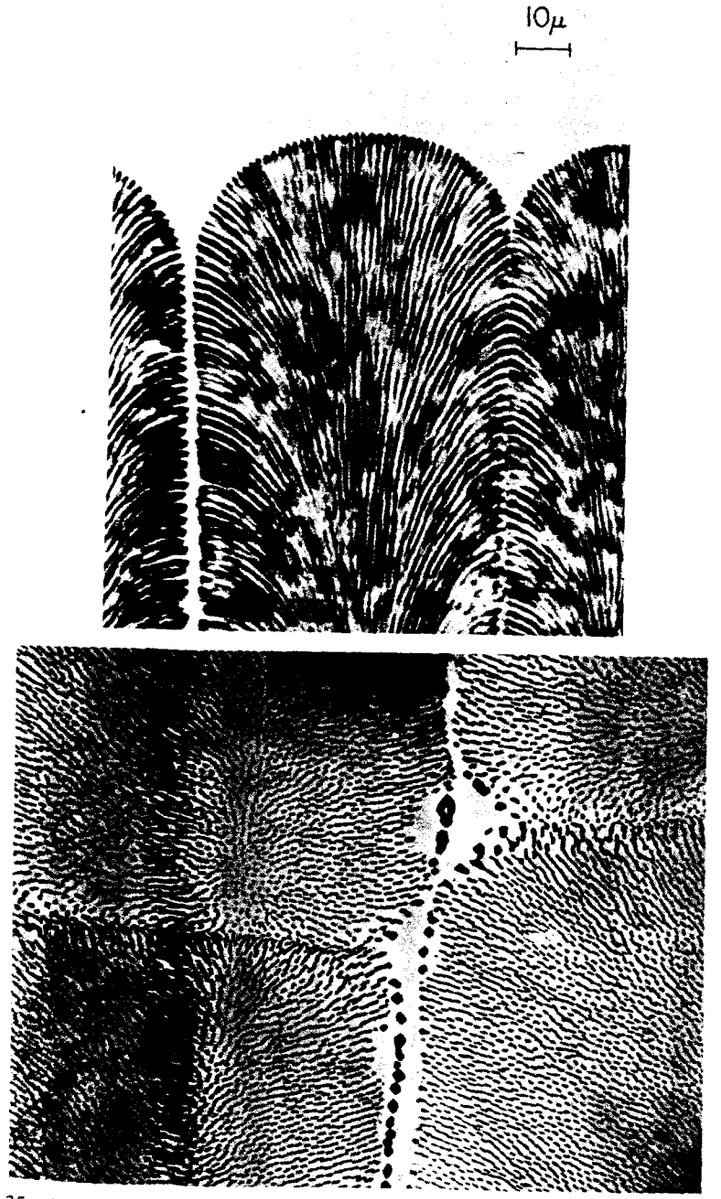

Fig. 4.35 (a) Cellular eutectic solidification front in a transparent organic alloy. (After J.D. Hunt and K.A. Jackson, *Transactions of the Metallurgical Society of AIME* **236** (1966) 843) (b) Transverse section through the cellular structure of an Al–Al_6Fe rod eutectic (3500). (Courtesy of J. Strid, University of Luleå, Sweden.)

where k_2 is another proportionality constant. This equation shows that by varying the interface undercooling (ΔT_0) it is possible to vary the growth rate (v) and spacing (λ) independently. It is therefore impossible to predict the spacing that will be observed for a given growth rate. However, controlled growth experiments show that a specific value of λ is always associated with a given growth rate. Examination of Equation 4.43 shows that when $\lambda = 2\lambda^*$, the growth rate is a maximum for a given undercooling, or, alternatively, the required undercooling is a minimum for a given growth rate. If it is assumed that growth occurs under these optimum conditions the observed spacing $\lambda_0 = 2\lambda^*$ and the observed growth rate is given by

$$v_0 = k_2 D \Delta T_0 / 2\lambda^{\infty 0}$$

However, from Equation 4.39, it is seen that $\Delta T_0 \propto 1/\lambda^*$ so that the following relationships are predicted:

$$v_0 \lambda_0^2 = k_3 \text{ (constant)} \tag{4.44}$$

and

$$\frac{v_0}{(\Delta T_0)^2} = k_4 \text{ (constant)} \tag{4.45}$$

There is in fact no physical basis for choosing $\lambda = 2\lambda^*$ and similar expressions can also be obtained using other assumptions concerning the spacing. Equations 4.44 and 4.45 are often found to be obeyed experimentally. For example measurements on the lamellar eutectic in the Pb–Sn system[10] show that $k_3 \sim 33\ \mu m^3\ s^{-1}$ and $k_4 \sim 1\ \mu m\ s^{-1}\ K^{-2}$. Therefore for a solidification rate of $1\ \mu m\ s^{-1}$, $\lambda_0 \sim 5\ \mu m$ and $\Delta T_0 \sim 1$ K.

The total undercooling at the eutectic front (ΔT_0) has two contributions, i.e.

$$\Delta T_0 = \Delta T_r + \Delta T_D \tag{4.46}$$

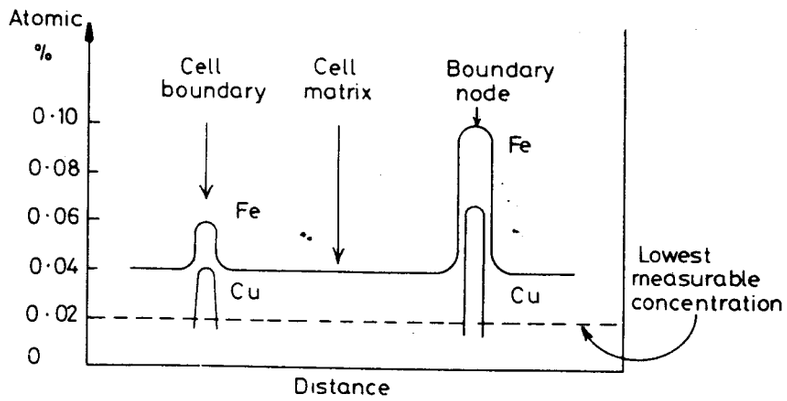

Fig. 4.36 Composition profiles across the cells in Fig. 4.35b.

ΔT_r is the undercooling required to overcome the interfacial curvature effects and ΔT_D is the undercooling required to give a sufficient composition difference to drive the diffusion. (Strictly speaking a ΔT_i term should also be added since a driving force is required to move the atoms across the interfaces, but this is negligible for high mobility interfaces.) A better theoretical treatment of eutectic solidification should take into account the fact that the composition of the liquid in contact with the interface and therefore ΔT_D vary continuously from the middle of the α to the middle of the β lamellae. Since the interface is essentially isothermal (ΔT_0 constant) the variation of ΔT_D must be compensated by a variation in ΔT_r, i.e. the interface curvature will change across the interface[11].

A planar eutectic front is not always stable. If for example the binary eutectic alloy contains impurities, or if other alloying elements are present, the interface tends to break up to form a cellular morphology. The solidification direction thus changes as the cell walls are approached and the lamellar or rod structure fans out and may even change to an irregular structure, Fig. 4.35. The impurity elements diffuse laterally and concentrate at the cell walls. In the case of the Al_6Fe—Al rod-like eutectic shown in Fig. 4.35 the impurity causing the cellular structure is mainly copper. Figure 4.36 shows how the concentration of copper and iron in the aluminium matrix increases in the cell walls and boundary nodes.

Cell formation in eutectic structures is analogous to that in single-phase solidification, and under controlled conditions it is possible to stabilize a planar interface by solidifying in a sufficiently high temperature gradient.

4.3.3 *Off-Eutectic Alloys*

When the bulk alloy composition (X_0) deviates from the equilibrium eutectic composition (X_E) as shown in Fig. 4.37 solidification usually begins close to T_1 with the formation of primary (α) dendrites. As the dendrites thicken solute is rejected into the remaining liquid until its composition reaches X_E and the eutectic solidifies. Under steady-state unidirectional solidification conditions in the presence of a shallow temperature gradient the solidification front could appear as in Fig. 4.37b. The tips of the dendrites are close to T_1 and the eutectic front, most probably cellular, close to T_E. Similar behaviour is found during the solidification of castings and ingots. In the absence of solid-state diffusion the centres of the dendrites, which solidified close to T_1, will contain less solute than the outer layers that solidify at progressively lower temperatures. This leads to what is known as *coring* in the final microstructure, Fig. 4.38. The eutectic does not always solidify as a two-phase mixture. When the volume fraction of one of the phases in the microstructure is very small it can form a so-called *divorced eutectic*. The minor phase then often appears as isolated islands and the other phase forms by the thickening of the dendrites.

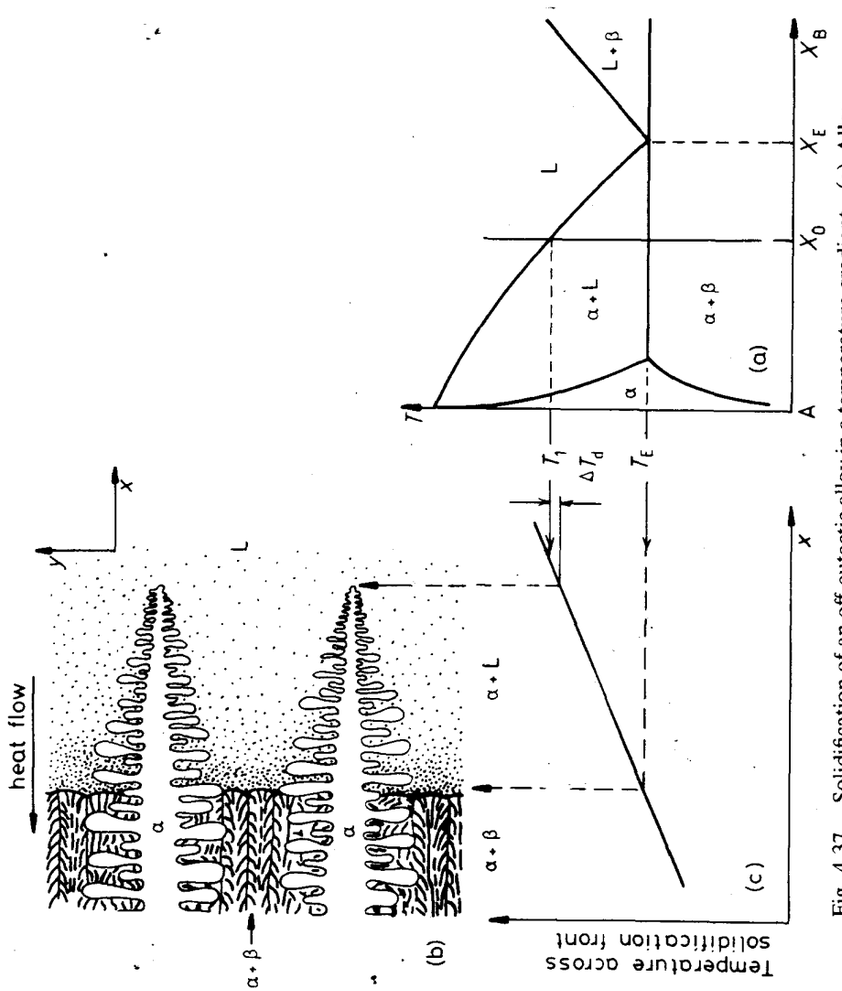

Fig. 4.37. Solidification of an off-eutectic alloy in a temperature gradient. (a) Alloy composition in relation to the phase diagram. (b) Schematic solidification front. (c) Temperature variation across solidification front (isotherms normal to x).

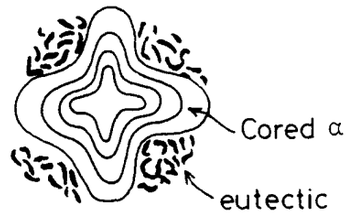

Fig. 4.38 Transverse section through a dendrite in Fig. 4.37.

Under controlled solidification conditions, e.g. in unidirectional solidification experiments, it is possible to solidify an off-eutectic alloy without permitting the formation of the primary dendritic phase. If the temperature gradient in the liquid is raised above a critical level the dendrite tips are overgrown by the eutectic and the alloy solidifies as 100% 'eutectic' with an overall composition X_0 instead of X_E. A similar change can be brought about if the growth rate is raised above a critical level. In both cases the reason for the disappearance of the primary dendrites is that for a given growth velocity the eutectic is able to grow at a higher temperature than the dendrite tips[12]. This phenomenon is of special interest in the production of *in situ* composite materials because the volume fraction of the two phases in the composite can be controlled by the choice of X_0[13].

4.3.4 *Peritectic Solidification*[14]

A typical phase diagram containing a peritectic reaction, i.e. $L + \alpha \rightarrow \beta$, is shown in Fig. 4.39a. During equilibrium solidification solid α with composition 'a' and liquid with composition 'c' react at the peritectic temperature T_p to give solid β of composition 'b'. However, the transformation rarely goes to completion in practice.

Consider for example the solidification of an alloy X_0 at a finite velocity in a shallow temperature gradient, Fig. 4.39b and c. As the temperature decreases the first phase to appear is α with the composition $\sim kX_0$ at a temperature close to T_1. α grows dendritically with successive layers solidifying at compositions determined by the local temperature and the α solidus. If diffusion in the dendrites is slow the liquid will eventually reach point c in Fig. 4.39a and on further cooling it reacts with the α to produce a layer of β. However, the α dendrites are then often effectively isolated from further reaction and are retained to lower temperatures. Meanwhile the β phase continues to precipitate from the liquid at compositions which follow the line bd. Again if there is no diffusion in the solid the liquid will finally reach point e and solidify as a $\beta + \gamma$ eutectic. The final solidified microstructure will then consist of cored α dendrites surrounded by a layer of β and islands of $\beta + \gamma$ eutectic, or divorced eutectic.

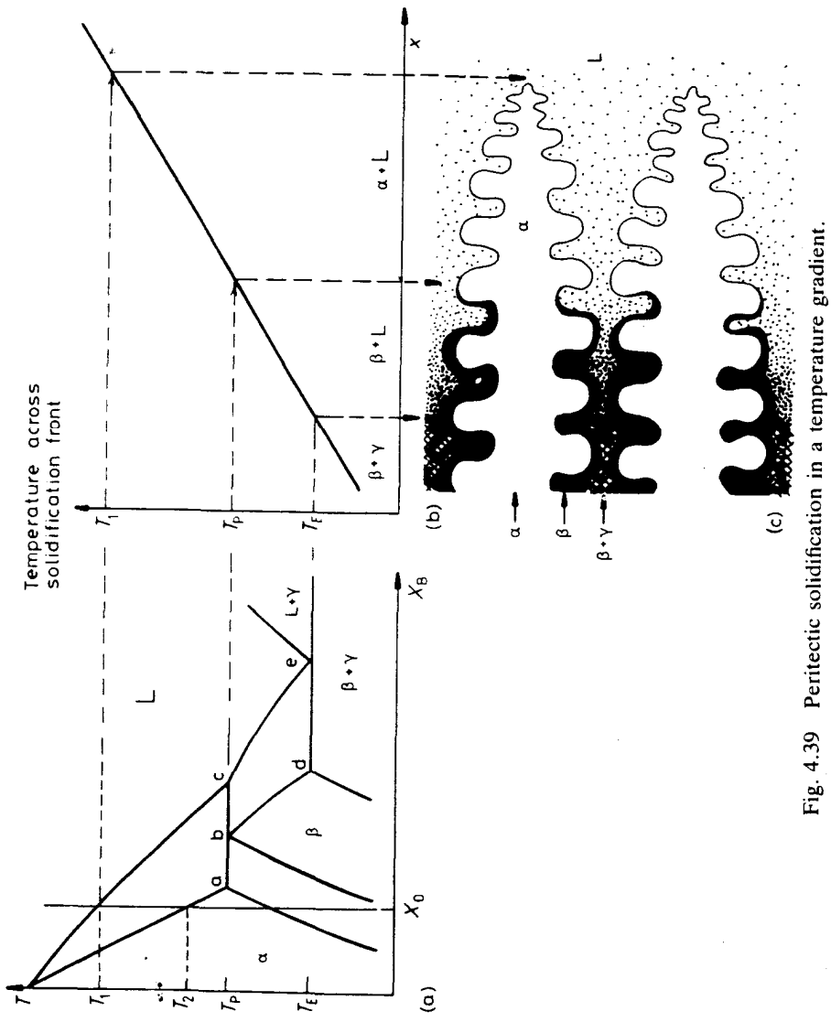

Fig. 4.39 Peritectic solidification in a temperature gradient.

If alloy X_0 were directionally solidified at increasing values of (T'_L/v) the temperature of the dendrite tips would progressively fall from T_1 towards T_2 (Fig. 4.39a) while the temperature at which the last liquid solidifies would increase towards T_2. Finally, solidification would take place behind a planar front at a temperature T_2, as discussed earlier in Section 4.3.1.

Planar-front solidification can also be obtained for alloys beyond 'a' in Fig. 4.39, provided a sufficiently high temperature–gradient/velocity ratio is used. Alloys between a and b then solidify with a 'eutectic-like' α + β structure. (The structure is better described as *composite* to avoid confusion concerning the term eutectic). Between b and d single-phase β forms, and beyond d β + γ eutectic-like structures can be formed.

The Fe—C phase diagram also contains a peritectic, Fig. 4.53a. However due to the high diffusivity of carbon at these high temperatures the peritectic reaction is very rapid and is able to convert all of the primary (δ) dendrites into the more stable austenite.

4.4 Solidification of Ingots and Castings

This section is concerned with technological applications of the theory of solidification, as developed earlier. Two of the most important applications are casting and weld solidification and we shall first consider these. In modern constructions there is a tendency towards the use of stronger, heavier sections welded with higher energy techniques and faster speeds. It is thus important for the physical metallurgist to consider the effect of the various solidification parameters on the microstructure and properties of fusion welds. This will then be followed by some selected case studies of as-solidified or as-welded engineering alloys and weld metals.

Most engineering alloys begin by being poured or cast into a fireproof container or *mould*. If the as-cast pieces are permitted to retain their shape afterwards, or are reshaped by machining, they are called *castings*. If they are later to be worked, e.g. by rolling, extrusion or forging, the pieces are called *ingots*, or *blanks* if they are relatively small. In either case the principles of solidification, and the requirements for high density and strength are the same. The moulds used in casting are often made of a material that can be remoulded or discarded after a casting series, such as sand. In the case of long casting series or ingot casting, however, the mould is of a more permanent material such as cast iron. The technological aspects of pouring and casting will not be dealt with here, but we shall confine our discussion simply to the mechanics of solidification of metals in a mould.

4.4.1 Ingot Structure

Generally speaking three different zones can be distinguished in solidified alloy ingots, Fig. 4.40. These are (i) an outer *chill zone* of equiaxed crystals, (ii) a *columnar zone* of elongated or column-like grains, and (iii) a central *equiaxed zone*.

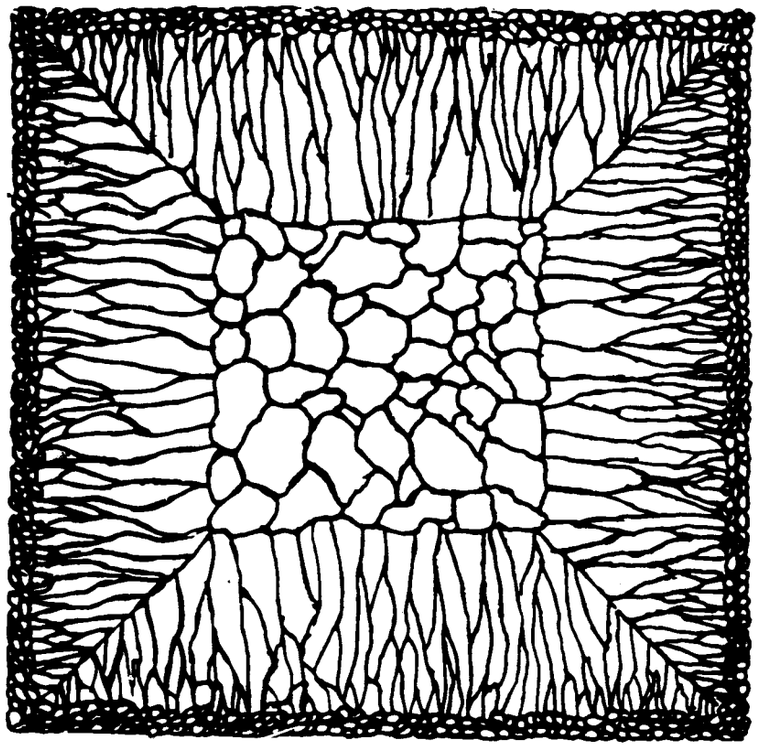

Fig. 4.40 Schematic cast grain structure. (After M.C. Flemings, *Solidification Processing*, McGraw-Hill, New York, 1974.)

Chill Zone

During pouring the liquid in contact with the cold mould wall is rapidly cooled below the liquidus temperature. Many solid nuclei then form on the mould wall and begin to grow into the liquid, Fig. 4.41. As the mould wall warms up it is possible for many of these solidified crystals to break away from the wall under the influence of the turbulent melt. If the pouring temperature is low the whole of the liquid will be rapidly cooled below the liquidus temperature and the crystals swept into the melt may be able to continue to grow. This is known as 'big-bang' nucleation since the liquid is immediately filled with a myriad of crystals. This produces an entirely equiaxed ingot structure, i.e. no columnar zone forms. If the pouring temperature is high, on the other hand, the liquid in the centre of the ingot will remain above the liquidus temperature for a long time and consequently the majority of crystals soon remelt after breaking away from the mould wall. Only those crystals remaining close to the wall will be able to grow to form the chill zone.

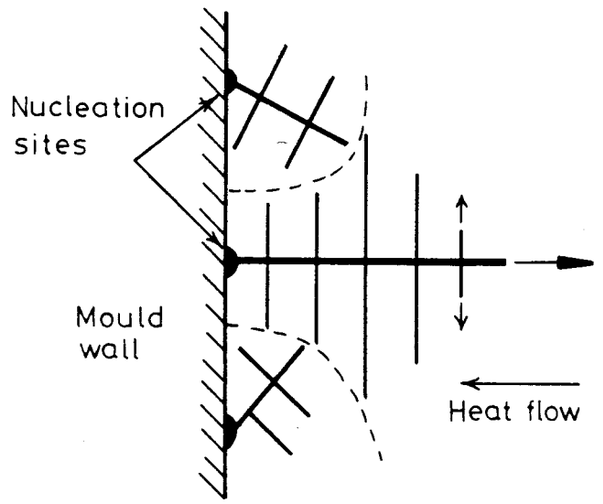

Fig. 4.41 Competitive growth soon after pouring. Dendrites with primary arms normal to the mould wall, i.e. parallel to the maximum temperature gradient, outgrow less favourably oriented neighbours.

Columnar Zone

Very soon after pouring the temperature gradient at the mould walls decreases and the crystals in the chill zone grow dendritically in certain crystallographic directions, e.g. ⟨100⟩ in the case of cubic metals. Those crystals with a ⟨100⟩ direction close to the direction of heat flow, i.e. perpendicular to the mould walls, grow fastest and are able to outgrow less favourably oriented neighbours, Fig. 4.42. This leads to the formation of the columnar grains all

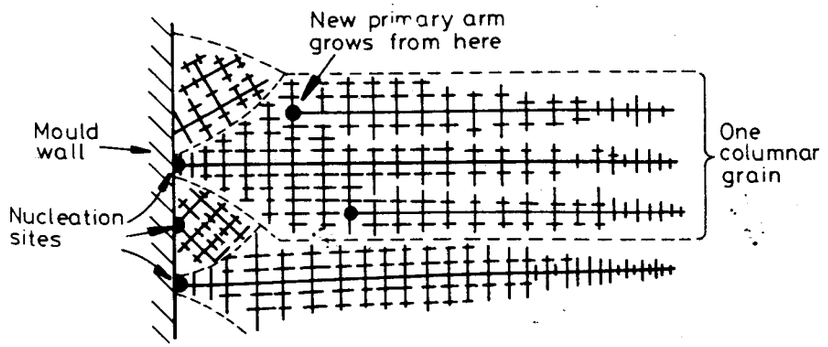

Fig. 4.42 Favourably oriented dendrites develop into columnar grains. Each columnar grain originates from the same heterogeneous nucleation site, but can contain many primary dendrite arms.